Journal of Nuclear Materials 408 (2011) 96–101

Contents lists available at ScienceDirect

Journal of Nuclear Materials

journal homepage: www.elsevier.com/locate/jnucmat

A novel procedure employing laser ultrasound technique and simplex algorism for the characterization of mechanical and geometrical properties in Zircaloy tubes with different levels of hydrogen charging

I-Hung Liu [a], Che-Hua Yang [b,*]

[a] Graduate Institute of Manufacturing Technology, National Taipei University of Technology, Taipei, Taiwan
[b] Graduate Institute of Mechanical and Electrical Engineering, National Taipei University of Technology, Taipei, Taiwan

ARTICLE INFO

Article history:
Received 24 August 2008
Accepted 5 November 2010

ABSTRACT

In this research, a procedure employing a laser ultrasound technique (LUT) and an inversion algorism is reported for nondestructive characterization of mechanical and geometrical properties in Zircaloy tubes with different levels of hydrogen charging. With the LUT, guided acoustic waves are generated to propagate in the Zircaloy tubes and are detected remotely by optical means. By measuring the dispersive wavespeeds followed by the inversion algorism, mechanical properties such as elastic moduli and geometrical property such as wall-thickness of Zircaloy tubes are characterized for different levels of hydrogen charging. Having the advantages of remote, non-contact and point-wise generation/detection, the reported procedure serves as a competitive candidate for the characterization of Zircaloy tubes generally operated in irradiative and temperature-elevated environments.

1. Introduction

Hydride induced hydrogen embrittlement in Zircaloy cladding tubes is reported to be responsible for the tube's degradation in mechanical properties while in reactor service [1]. The degree of embrittlement was reported to be affected mainly by hydrogen concentration (HC) [2]. Many methods, destructive or nondestructive, have been developed for HC characterizations. Hot vacuum extraction mass spectrometry (HVEMS) [3], inert-gas fusion (IGF) [4] and quantitative metallography [5] have been employed for destructive HC characterization. While nondestructive HC characterization is desired, researches based on eddy current technique [6], neutron radiography [7], and ultrasound techniques [8] are continuously been reported.

In a previous study, an ultrasound-based technique employing a low-frequency acoustic microscope was reported for nondestructive HC characterization in Zircaloy cladding tubes [9]. Recently, another inspection method known as laser ultrasound technique (LUT) was reported for the HC characterization [10]. Using optical methods for the generation and detection of ultrasonic waves [11,12], LUT offers advantages of remote and non-contact ultrasonic inspections over traditional piezoelectric transducers and can be applied to the inspections in hostile or inaccessible environments. The generation mechanism of elastic waves with a pulsed laser is shown in Fig. 1, where the laser's electromagnetic energy is partially absorbed by the sample's surface and further converted to thermal expansion to generate ultrasonic waves [13]. The laser optical probe used to detect the ultrasonic motions can be a knife-edge probe [14,15], a heterodyne Michelson-type interferometer [16], a Fabry–Perot interferometer [17], or a photorefractive interferometer [18]. Each of these optical probes exhibits individual advantage over others, depending on the interested applications. Since the LUT was introduced in 1980s, it has been successfully applied to many application areas involved with nondestructive inspection [19,20], material characterization [9,10,21], and other fundamental researches in ultrasonics [22].

It is much more valuable if some of the major mechanical or geometrical properties can be accessed while the inspection process is completed. To extract useful properties from measured ultrasound data, inversion procedures based on simplex algorism are generally employed. In 1965, Nelder and Mead proposed a simplex method for solving minimum solution [23]. Since then, the simplex method has been applied to solve regression curve [24]. In the area of ultrasound inspection, the simplex method was applied to obtain mechanical properties from leaky Lamb wave measurements on composite materials [25], to calculate material properties of thin film from measurements with scanning acoustic microscope (SAM) [26], and to characterize material properties of two-layered Zircaloy tubes [27].

* Corresponding author.
E-mail addresses: t5669007@ntut.edu.tw (I.-H. Liu), chyang@ntut.edu.tw (C.-H. Yang).

0022-3115/$ - see front matter © 2010 Elsevier B.V. All rights reserved.
doi:10.1016/j.jnucmat.2010.11.018

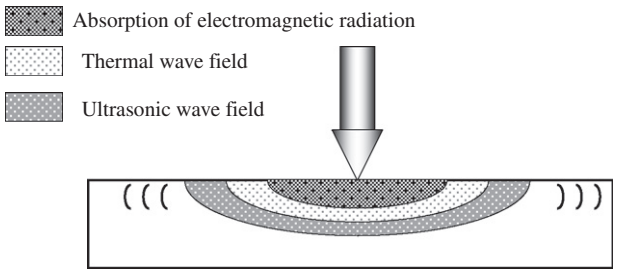

Fig. 1. A schematic showing the generation mechanism of ultrasonic waves with a pulsed laser (after Scruby and Drain [11]).

In this research, a novel procedure employing LUT together with a simplex-based inversion algorism is reported to characterize properties of Zircaloy tubes with different levels of hydrogen charging. Details of the current study are described in the following sections.

2. Zircaloy samples

Zircaloy-4 tube specimens were hydrogen-charged by Institute of Nuclear Research (INER) to three target HCs by weight of 200 ppm (labeled as FCR02), 500 ppm (labeled as FCR05) and 1200 ppm (labeled as FCR12). With smooth surface condition, these Zircaloy samples have outer radius of about 5.4 mm, thickness of about 0.6 mm and 60 mm in length. The specimens were hydrogen-charged by a thermal cycling process. After oxide removal operation in an argon atmosphere, the Zircaloy specimen was encapsulated with a pre-determined amount of purified hydrogen in a Pyrex capsule of sufficient volume such that a low hydrogen partial pressure could be obtained to avert the formation of hydride layers. The encapsulated Zircaloy specimen was then thermally cycled between 90 °C and hydriding temperatures for a certain number of cycles, depending on the target HC level. The hydriding temperature starts at a temperature of about 180 °C, which increases with an increment of 10 °C for succeeding cycles up to 300 °C. Precautions against re-oxidation of the surface-treated Zircaloy specimens were exercised before completion of the encapsulation operation.

Hydrogen concentration of the hydrided Zircaloy specimens were determined by an inert-gas fusion method using a LECO RH-404 hydrogen determinator. The measured HCs for the three hydrogen-charged samples are listed in Table 1, where the averaged HC for the FCR02 sample is 209 ppm, 428 ppm for the FCR05, and 1070 ppm for the FCR12, respectively. Also, the hydrided Zircaloy specimens were examined with optical microscopy to reveal the hydride morphology. Fig. 2 shows micrographs for the three Zircaloy samples with different HCs. It is shown that precipitated hydrides are circumferentially orientated and evenly distributed along the thickness and circumferential directions. While the HC increasing, more precipitated hydride can be observed in the micrographs. The Zircaloy samples are then tested with LUT in the air at room temperature for further material characterizations. An archive Zircaloy sample without hydrogen charging is also tested for a comparison with the hydrogen-charged samples.

Table 1
Measured HCs for the Zircaloy samples.

Sample	Average HC (ppm)	Standard deviation
Archive	0	0
FCR02	209	5
FCR05	428	22
FCR12	1070	81

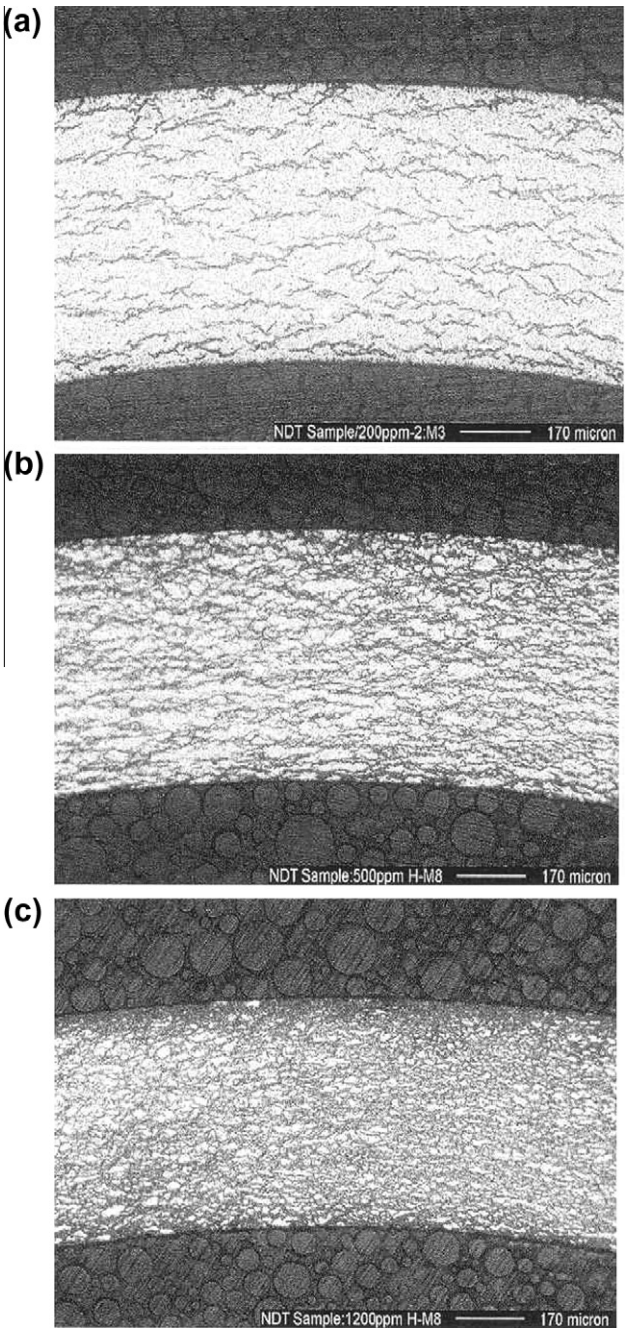

Fig. 2. Optical micrographs for the hydrogen-charged Zircaloy samples: (a) FCR02, (b) FCR05 and (c) FCR12.

3. Laser ultrasound technique

A laser ultrasound technique (LUT) is used for the measurement of dispersion spectra of guided acoustic waves propagating in the Zircaloy tubes. Fig. 3 shows a schematic for the experimental configuration of the LUT system. The LUT system includes a pulsed Nd:YAG laser, an interferometer, a scanning stage, and a computer with fast A/D converter. The pulsed Nd:YAG laser (Quantel YG780) with a wavelength of 532 nm, a duration time of 6.6 ns, and an energy of about 100 mJ is used for the generation of ultrasonic waves. The interferometer (Polytec OFV 511) used for the non-contact detection of ultrasound is a heterodyne interferometer with a detection bandwidth of 30 MHz. The scanning stage controlled by the computer drives a mirror to scan the Nd:YAG laser beam along

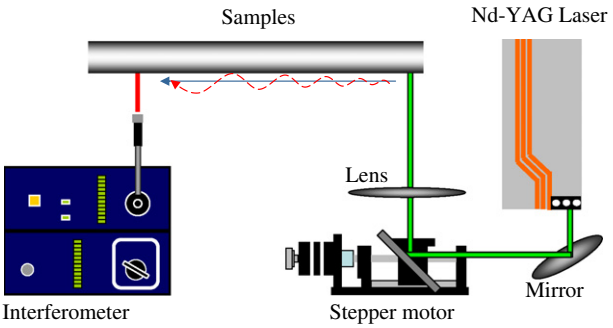

Fig. 3. A schematic showing the experimental configuration of laser ultrasound system.

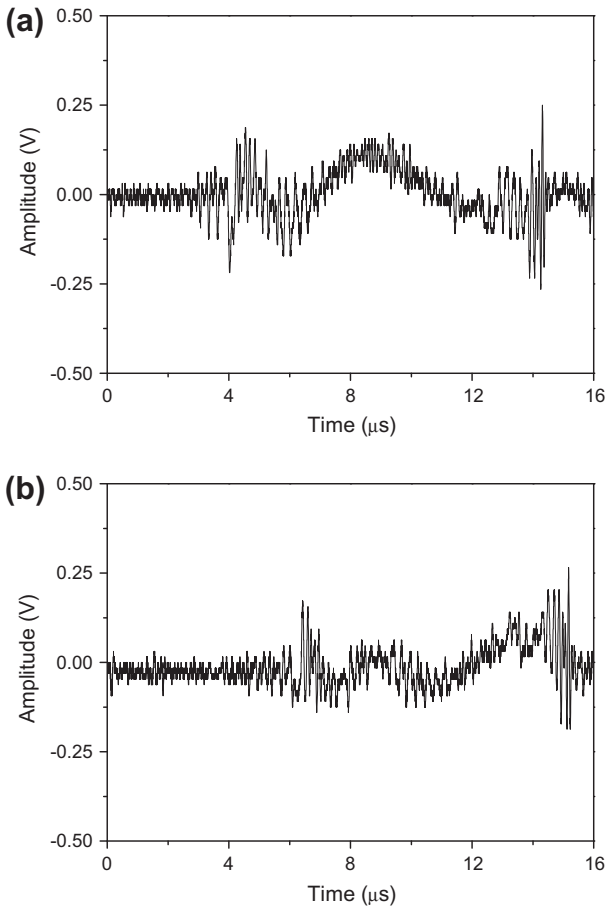

Fig. 4. Time-domain waveforms measured with the LUT while the generation and reception positions are separated axially by distances of (a) 9.4 mm, and (b) 14.4 mm on the surface of the archive sample.

the axial direction of the Zircaloy tubes. The computer with a fast A/D converter is used for controlling the scanning stage, waveform acquisition, and signal processing.

Figs. 4a and b show time-domain waveforms measured with the LUT while the generation and reception positions are separated axially by distances of 9.4 mm and 14.4 mm on the surface of the archive sample, respectively. The LUT-generated guided waves propagating in Zircaloy tubes are dispersive, meaning the phase velocity is a function of the frequency. To measure the dispersion relation of the guided waves propagating in the Zircaloy tubes, a B-scan scheme followed by a two-dimensional fast Fourier transform (2D-FFT) signal processing is adopted. For the B-scan, the impinging spot of generation laser is initially placed near the

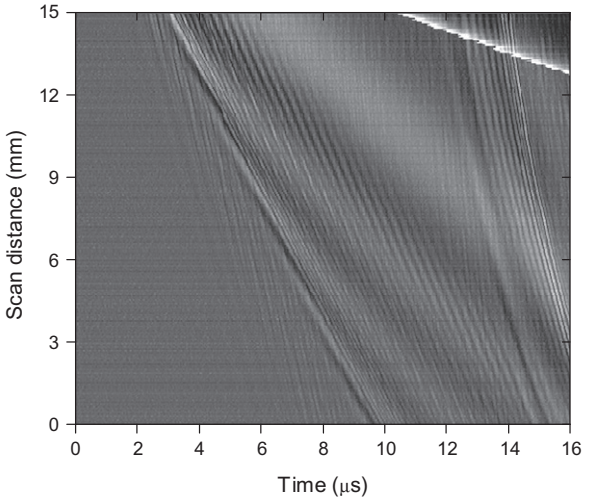

Fig. 5. B-scan data measured with the LUT for the archive Zircaloy tube.

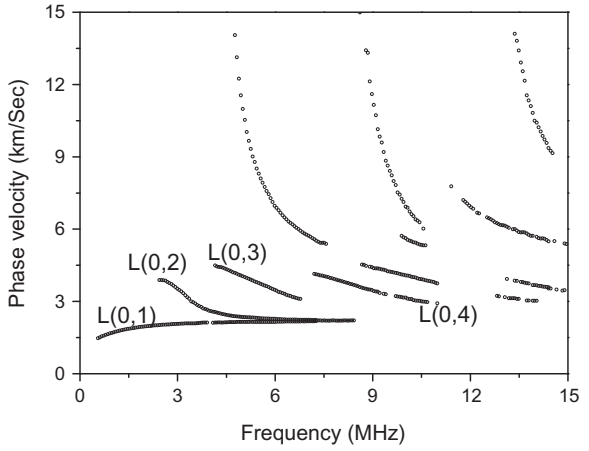

Fig. 6. Measured dispersion curves for the archive Zircaloy sample.

illuminated spot of the interferometer by a distance of about 5 mm, and then scanned away. A total scanning distance of 15 mm in 300 steps is used to obtain a set of dispersion spectra. After the waveforms at each step are collected, a set of B-scan data for the archived sample is shown in a gray scale format in Fig. 5. In this figure, the horizontal axis denotes the elapsed time, the vertical axis denotes the scanning position, and the gray scale represents the relative amplitude of acoustic waves. Multi-mode dispersion spectra are further extracted from the B-scan data by the 2D-FFT signal processing. In the 2D-FFT, the first FFT is taken with respect to time, and the second FFT with respect to the scanning position. The 2D-FFT transforms the B-scan data into ultrasound amplitude as a function of frequency (f) and wavenumber (k). A peak-detection routine is used to find the trajectories of peak amplitude in the f–k space. Finally, the dispersion curves in the form of ultrasound phase velocity (V) versus frequency are obtained with the aid of the relation $V = 2\pi f/k$. Fig. 6 shows the measured dispersion spectra for the archive sample. The first four longitudinal guided modes are labeled as L(0, 1), L(0, 2), L(0, 3) and L(0, 4).

4. Inversion algorism

A simplex inversion procedure is employed to extract material and geometrical properties for the Zircaloy samples based on the

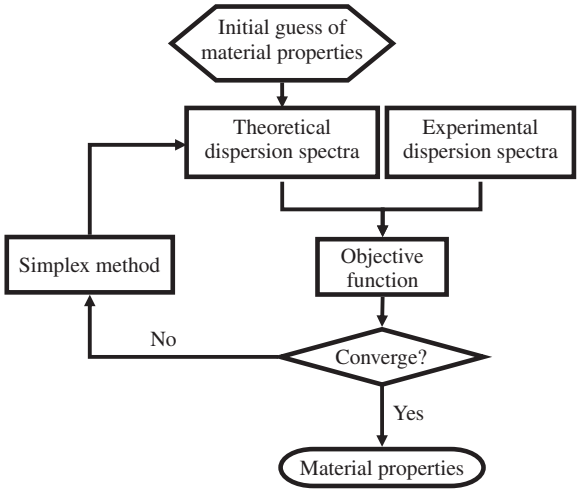

Fig. 7. A block diagram showing the inversion procedure.

LUT-measured dispersion spectra of guided modes propagating in tubes. The procedure based on the simplex algorism to extract properties from the measured dispersion spectra is illustrated in a block diagram in Fig. 7. In this algorism, the LUT-measured dispersion spectra are now used as a reference for a comparison with the theoretically calculated spectra with undetermined properties. The algorism starts by choosing five sets of initially guessed properties and adjusts the properties recursively until a tolerance is met to determine a set of properties. The determined properties represent for the properties obtained with the proposed inversion procedure.

Theoretical models for calculating dispersion spectra of guided waves propagating in a tube can be expresses as:

$$D_3 = \begin{vmatrix} C_{11} & C_{12} & C_{14} & C_{15} \\ C_{31} & C_{32} & C_{34} & C_{35} \\ C_{41} & C_{42} & C_{44} & C_{45} \\ C_{61} & C_{62} & C_{64} & C_{65} \end{vmatrix} = 0. \quad (1)$$

Here the matrix coefficients C_{ij} ($i = 1, \ldots, 6$, $j = 1, \ldots, 6$) can be referred to Refs. [28,29].

An objective function defined in the following equation is used as a measure of error between the calculated and measured dispersion spectra:

$$f_{obj} = \sum_{i=1}^{n} \left[v(f_i)^{Exp} - v(f_i)^{Th} \right]^2. \quad (2)$$

In Eq. (2), there is a total of n points selected for the evaluation of objective function f_{obj}. For each point with a frequency f_i, the measured and calculated velocities are represented as $v(f_i)^{Exp}$ and $v(f_i)^{Th}$, respectively. The objective function is defined as the square sum of difference between the measured and calculated phase velocities.

A benchmark test is performed before the inversion procedure is used to determine properties from LUT measurement. Purpose of performing the benchmark test is to test the convergence of the procedure related to the objective function, and not covering the effects of noise in the LUT data. In this benchmark test, the measured dispersion spectra in Fig. 7 are fed with a set of dispersion spectra calculated using the theoretical model by substituting a set of prescribed properties. The procedure is then used to invert, or back-calculate, the properties, which are then compared with the prescribed properties. Quality of inversion algorism can be evaluated by checking the agreement between the inverted properties and the prescribed properties. In the determination of

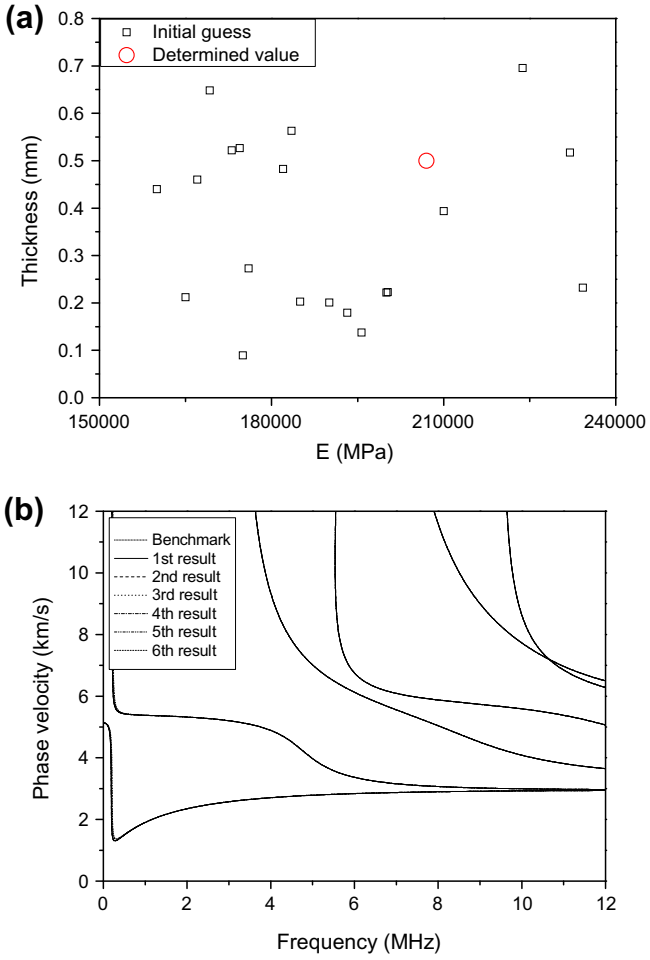

Fig. 8. (a) Convergence test in the t–E subspace showing the determined properties agreeing well with the prescribed values, (b) dispersion curves calculated with the prescribed properties and various inverted properties.

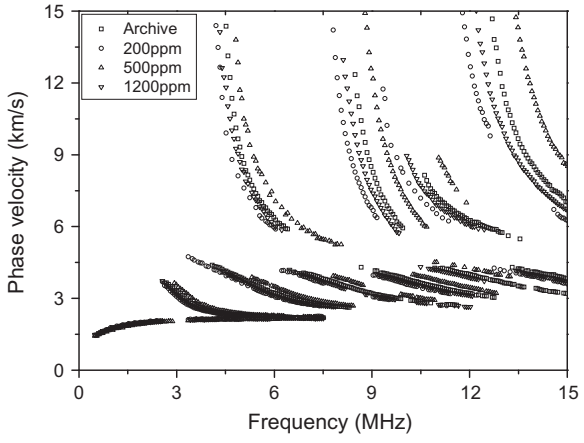

Fig. 9. Measured dispersion curves for all the four Zircaloy samples.

guided waves dispersion spectra, there are five independent properties, namely, Young's modulus (E), Poisson's ratio (v), mass density (ρ), inner radius (IR) and outer radius (OR). Note that the wall-thickness (t) is related to IR and OR by the relation $t = OR - IR$. Also, the dispersion spectra is very sensitive to t, however, not sensitive to IR or OR. In this benchmark test, $\rho = 7.85$ g/cm^3 is fixed while the

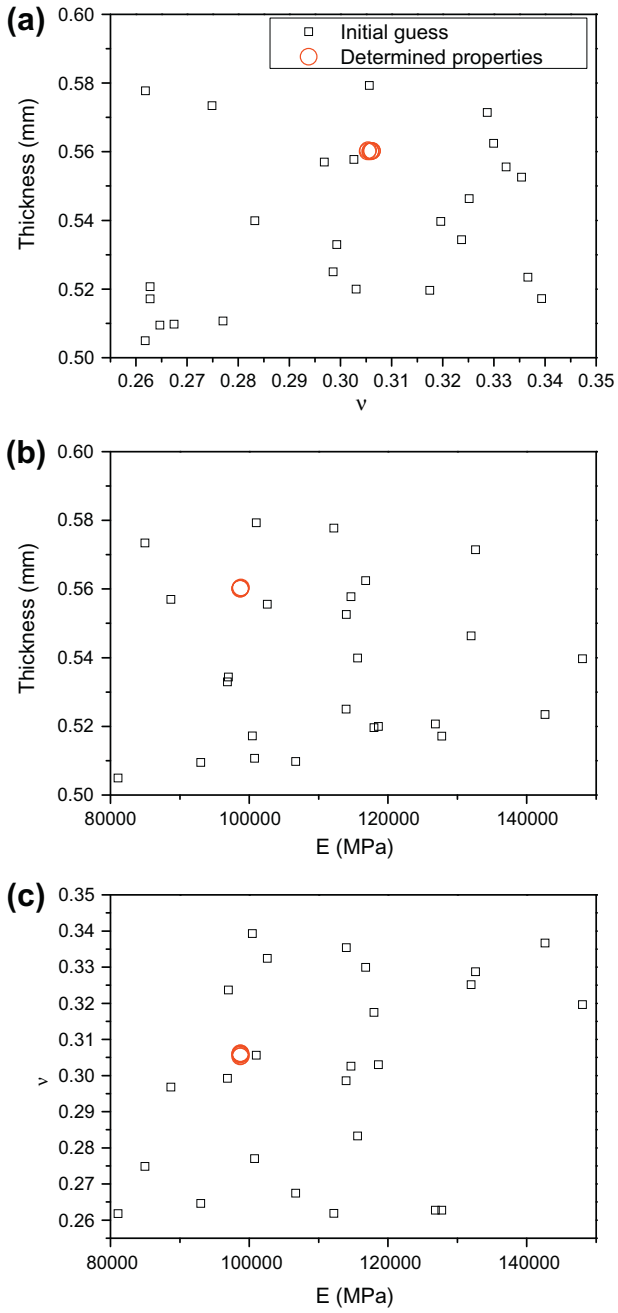

Fig. 10. Initial and determined properties in (a) t–ν, (b) t–E, and (c) ν–E subspaces.

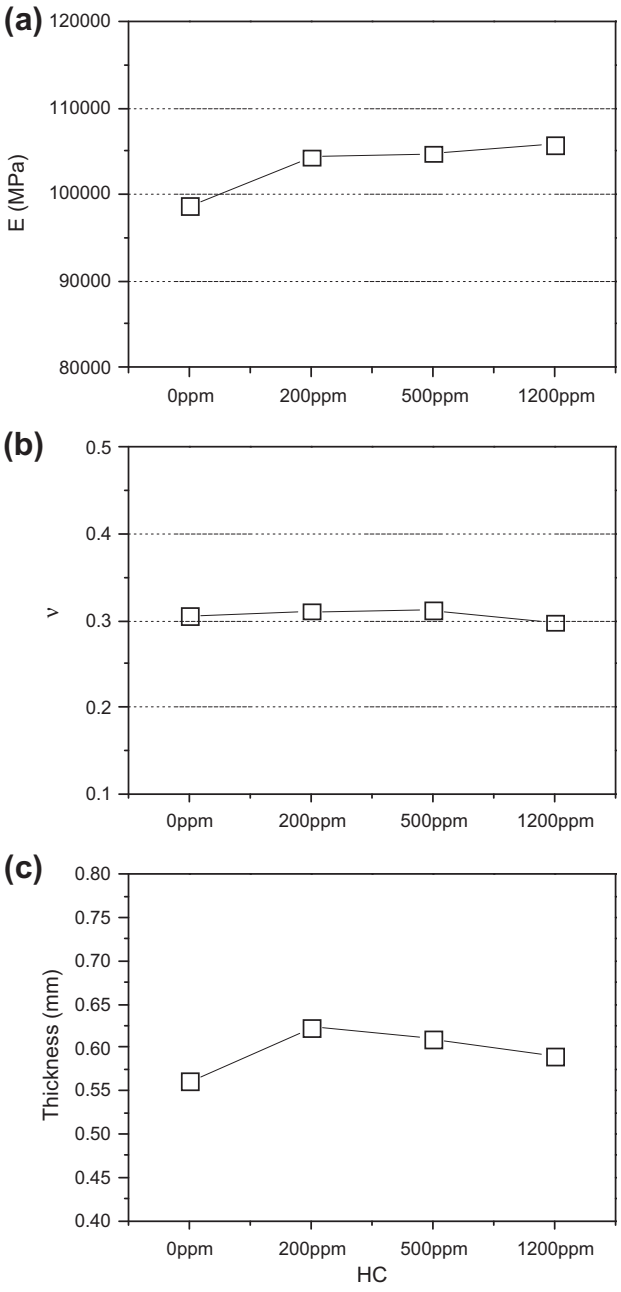

Fig. 11. Inverted values on (a) E, (b) ν, and (c) t as a function of HC.

inversion procedure is used to determine the other four properties, E, ν, t, and OR. A set of prescribed properties are given as $E = 207$ GPa, $\nu = 0.3$, $t = 0.5$ mm, and $OR = 5$ mm. The prescribed properties signify a steel tube without texture. However, this algorism is also valid for Zircaloy with precipitated hydride. Fig. 8a shows the six sets of initially guessed and determined properties in the t–E subspace while Fig. 8b shows the corresponding dispersion curves calculated by using the constants in Fig. 8a. The determined properties converge to values very close to the prescribed properties within 0.01%. Accordingly, the dispersion curves shown in Fig. 8b calculated with the determined constants agree well with the benchmark dispersion curves based on the prescribed properties. Results of the benchmark test advocate the reliability for the inversion procedure in extracting properties from the dispersion spectra.

5. Results and discussions

Fig. 9 shows the measured dispersion spectra with the LUT for the four Zircaloy samples with different HCs. Effects of hydrogen charging involving changes of various properties can be observed from the shifting of dispersion spectra for the four guided modes. It is noted that dispersion curves for the guided modes shift towards to the right, or the high frequency, while HC increases. Changes in properties associated with hydrogen charging governing the movement of dispersion spectra will be explored thorough the inverted properties form these LUT-measured spectra.

Inversion on the interested properties for the hydrogen-charged Zircaloy samples is based on the procedure in Fig. 7 and the measured dispersion spectra in Fig. 9. In this inversion process, mass densities (ρ) for the four samples are measured independently by using the Archimedes principle. There are three properties left

Table 2
Determined properties from the inversion process.

	Archive	FCR02	FCR05	FCR12
E (GPa)	98.7	104.3	104.7	105.7
v	0.306	0.311	0.310	0.298
Thickness (mm)	0.561	0.623	0.610	0.590

Table 3
A comparison on the inverted and measured wall-thickness.

Thickness	Archive	FCR02	FCR05	FCR12
Inversion	0.561	0.623	0.610	0.590
Calipers	0.56	0.63	0.61	0.58
Error (%)	0.18	1.17	0.08	1.77

for the inversion procedure to determine, namely, wall-thickness (t), Young's modulus (E), and Poisson's ratio (v). Fig. 10a–c show the initial and determined properties for the archive sample in the t–v, t–E, and v–E subspaces, respectively. The initial guessed values for t ranges from 0.5 to 0.6 mm, E from 80 GPa to 150 GPa, and v from 0.26 to 0.35. From each of these initial guessed values, the determined properties all converge to values near (t, E, v) = (0.561 mm, 98.7 GPa, 0.306). Fig. 10 suggests that the inversion process from the measured dispersion spectra to have consistent convergence.

Inverted properties from the measured dispersion spectra for the four Zircaloy samples are shown Fig. 11 with detailed numerical values in Table 2. Several clear trends can be summarized from this table as HC changes. Regarding to the elastic moduli, no clear trend can be observed for the Poisson's ratio (v). Inverted values of v for the four samples are 0.306, 0.311, 0.310, and 0.298. The inverted Young's modulus shows a clear trend that E increases as HC increases. E shows an obvious increase from 98.7 GPa for the archive sample to 104.3 GPa for FCR02, and keeps increasing to 104.7 GPa for FCR05 and 105.7 GPa for FCR12. It is further noted that wall-thickness for the four Zircaloy samples varies substantially as well. The thicknesses are 0.561 mm, 0.623 mm, 0.610 mm and 0.590 mm for the archive, FCR02, FCR05, and FCR12 samples, respectively. Independent measurements for the thicknesses of the four samples using calipers are listed in Table 3 for a comparison. The measured values are 0.56 mm, 0.63 mm, 0.61 mm and 0.58 mm. These two sets of thickness data show good agreement with low discrepancy ranging from 0.08% to 1.77%.

6. Conclusions

A procedure combining a laser ultrasound technique (LUT) and a simplex-based inversion algorism is reported to characterize material and geometrical properties of Zircaloy tubes with different levels of hydrogen charging. The reported procedure demonstrates its ability to obtain mechanical properties such as elastic moduli in a nondestructive way. In the meanwhile, geometrical properties such as wall-thickness of about 0.6 mm are characterized with a confirmed high precision of better than 1.77% in a remote way. The reported procedure is a remote, non-contact optical technique, and therefore is suitable to characterize Zircaloy tubes normally operated in irradiative and temperature-elevated environments. This procedure is under development for the characterization of inhomogeneous distribution of hydride across the thickness direction.

Acknowledgements

Financial support from National Science Council, Taiwan, through Grant No. NSC97-NU-7-182-003 is gratefully acknowledged. Also kindly discussions and efforts for sample preparations and hydrogen measurements by Dr. R.C. Kuo and Dr. C.T. Yang in Institute of Nuclear Research (INER), Taiwan, R.O.C. are acknowledged.

References

[1] C.E. Coleman, D. Hardie, Nature 208 (1965) 69–70.
[2] J.H. Huang, S.P. Huang, J. Nucl. Mater. 208 (1994) 166–179.
[3] A.N. Zaidel', E.P. Korennoi, Opt. Spectrosc. 10 (1961) 570–576.
[4] B.C. Park, Y. Kido, D. Accili, Biochemistry 38 (1999) 7517–7523.
[5] B.Z. Hyatt, Westinghouse Electric Corp. Report No. WAPD-TM-1431, 1982.
[6] A. Lois, H. Mendonca, M. Ruch, in: 15th World Conference on Nondestructive Testing, Roma, Italy, October 15–21, 2000.
[7] R. Yasuda, M. Matsubayashi, M. Nakata, K. Harada, J. Nucl. Mater. 302 (2002) 156.
[8] J.L. Singh, K.P. Prasannan, H.N. Singh, K.C. Sahoo, D.S.C. Purushotham, 7th European Conference on Non-Destructive Testing, Copenhagen, Denmark, May 26–29, 1998.
[9] C.H. Yang, M.F. Huang, J. Nucl. Mater. 335 (3) (2004) 359.
[10] C.H. Yang, Y.A. Lai, Key Eng. Mater. 321–323 (2006) 410–413.
[11] C.B. Scruby, L.E. Drain, Laser-Ultrasonics: Techniques and Applications, Adam Hilger, Bristol, UK, 1990.
[12] D.A. Hutchings, in: W.P. Mason, R.N. Thurston (Eds.), Physical Acoustics, vol. XVIII, Academic, New York, 1988.
[13] L.S. Gournay, J. Acoust. Soc. Am. 40 (1966) 1322.
[14] R.L. Whitman, A. Korpel, Appl. Opt. Lett. 8 (1969) 1567–1576.
[15] G.I. Stegeman, IEEE Trans. Son. Ultrason. SU-23 (1976) 33.
[16] G. Bouchard, D.B. Bogy, J. Acoust. Soc. Am. 77 (1985) 1003.
[17] J.P. Monchalin, Appl. Phys. Lett. 47 (1985) 14–16.
[18] A. Blouin, J.P. Monchalin, Appl. Phys. Lett. 65 (1994) 932.
[19] A.D.W. McKie, R.C. Addison Jr., Proc. SPIE 3397 (1998) 107.
[20] J.A. Rogers, M. Fuchs, M.J. Banet, J.B. Hanselman, R. Logan, A. Nelson, Appl. Phys. Lett. 71 (1997) 225–227.
[21] P.L. Ridgway, A.J. Hunt, M. Quinby-Hunt, R.E. Russo, Ultrasonics 37 (1999) 395.
[22] C.H. Yang, J.S. Liaw, Jpn. J. Appl. Phys. 39 (2000) 2741.
[23] J.A. Nelder, R. Mead, Comp. J. 7 (1965) 308–313.
[24] M.S. Caceci, W.P. Cacheris, Byte Mag. 9 (5) (1984) 340–362.
[25] M.R. Karim, A.K. Mal, J. Acoust. Soc. Am. 88 (1990) 482–491.
[26] O. Behrend, A. Kulik, G. Gremaud, Appl. Phys. Lett. 22 (1993) 2787–2789.
[27] I.H. Liu, C.H. Yang, in: 12th A-PCNDT 2006 Asia–Pacific Conf. on NDT, Auckland, New Zealand, November 5–10, 2006.
[28] C. Gazis, J. Acoust. Soc. Am. 31 (1959) 568–573.
[29] C. Gazis, J. Acoust. Soc. Am. 31 (1959) 573–578.